Physics in Medicine & Biology

IPEM Institute of Physics and Engineering in Medicine

PAPER

OPEN ACCESS

Vacuum ultraviolet silicon photomultipliers applied to BaF$_2$ cross-luminescence detection for high-rate ultrafast timing applications

S Gundacker[1,2,8] , R H Pots[1,3] , A Nepomnyashchikh[4], E Radzhabov[4], R Shendrik[4] , S Omelkov[5], M Kirm[5], F Acerbi[6], M Capasso[6,9], G Paternoster[6], A Mazzi[6], A Gola[6], J Chen[7] and E Auffray[1]

1 CERN,1211 Geneve 23, Switzerland
2 UniMIB,Piazza dell'Ateneo Nuovo, 1-20126, Milano, Italy
3 RWTH Aachen, Templergraben 55, 52062 Aachen, Germany
4 Vinogradov Institute of Geochemistry, Favorskii Street 1a, PO Box 4019, Irkutsk 664033, Russia
5 Institute of Physics, University of Tartu, W. Ostwald Str. 1, Tartu 50411, Estonia
6 Fondazione Bruno Kessler, via Sommarive 18, Trento 38123, Italy
7 Shanghai Institute of Ceramics, Chinese Academy of Sciences, 588 Hesuo Road, Jiading District, Shanghai 201899, People's Republic of China
8 Present address: Department of Physics of Molecular Imaging Systems, Institute for Experimental Molecular Imaging, RWTH Aachen University, Forckenbeckstrasse 55, 52074 Aachen, Germany.
9 Present address: Barnard College, Columbia University, 3009 Broadway, NY 10027-6909, United States of America.

E-mail: stefan.gundacker@pmi.rwth-aachen.de and stefan.gundacker@cern.ch

Abstract

Inorganic scintillators are widely used for fast timing applications in high-energy physics (HEP) experiments, time-of-flight positron emission tomography and time tagging of soft and hard x-ray photons at advanced light sources. As the best coincidence time resolution (CTR) achievable is proportional to the square root of the scintillation decay time it is worth studying fast cross-luminescence, for example in BaF$_2$ which has an intrinsic yield of about 1400 photons/MeV. However, emission bands in BaF$_2$ are located in the deep-UV at 195 nm and 220 nm, which sets severe constraints on photodetector selection. Recent developments in dark matter and neutrinoless double beta decay searches have led to silicon photomultipliers (SiPMs) with photon detection efficiencies of 20%–25% at wavelengths of 200 nm. We tested state-of-the-art devices from Fondazione Bruno Kessler and measured a best CTR of 51 ± 5 ps full width at half maximum when coupling 2 mm × 2 mm × 3 mm BaF$_2$ crystals excited by 511 keV electron–positron annihilation gammas. Using these vacuum ultraviolet SiPMs we recorded the scintillation kinetics of samples from Epic Crystal under 511 keV excitation, confirming a fast decay time of 855 ps with 12.2% relative light yield and 805 ns with 84.0% abundance, together with a smaller rise time of 4 ps beyond the resolution of our setup. The total intrinsic light yield was determined to be 8500 photons/MeV. We also revealed a faster component with 136 ps decay time and 3.7% light yield contribution, which is extremely interesting for the fastest timing applications. Timing characteristics and CTR results on BaF$_2$ samples from different producers and with different dopants (yttrium, cadmium and lanthanum) are given, and clearly show that the the slow 800 ns emission can be effectively suppressed. Such results ultimately pave the way for high-rate ultrafast timing applications in medical diagnosis, range monitoring in proton or heavy ion therapy and HEP.

1. Introduction

Cross-luminescence emission in BaF$_2$ is known to be very fast, with a ∼600 ps decay time component having a light yield of ∼1400 photons/MeV (Ershov *et al* 1982, Laval *et al* 1983, Aleksandrov *et al* 1984). Hence, BaF$_2$ is an excellent candidate for fastest timing in certain positron emission tomography (PET) concepts and high-energy physics (HEP) (Hu *et al* 2019) due to its high density. However, the fast cross-luminescence emission is a true
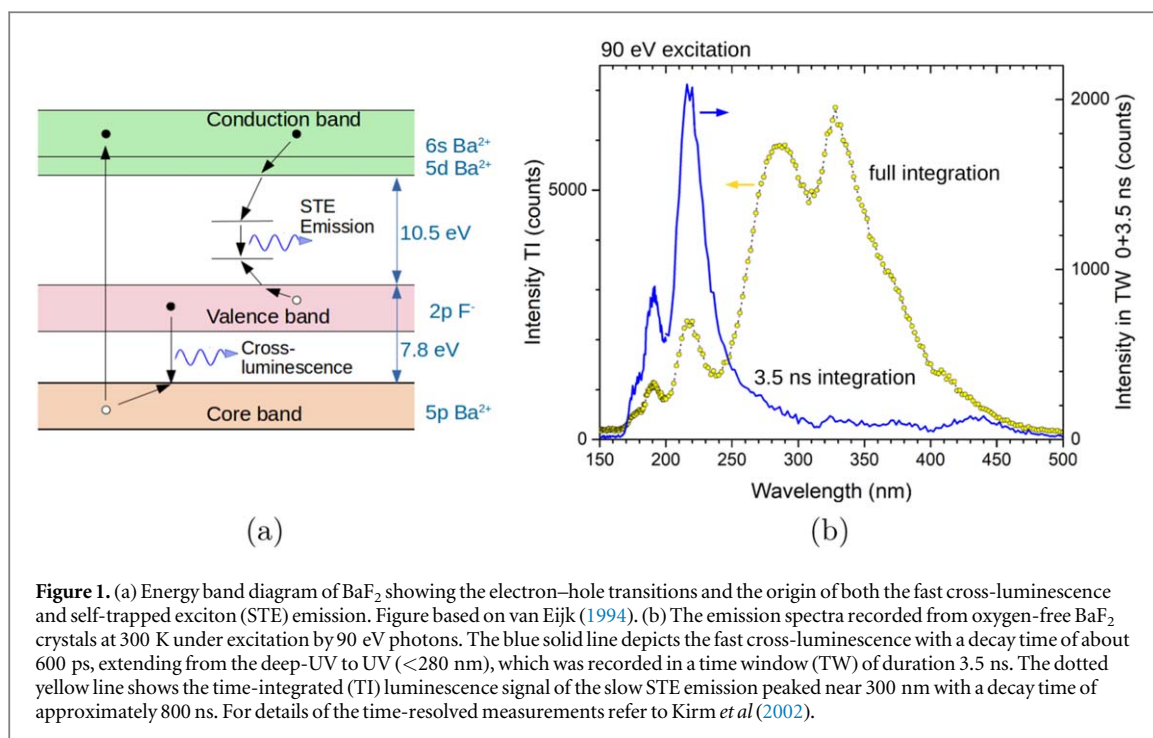
Figure 1. (a) Energy band diagram of BaF$_2$ showing the electron–hole transitions and the origin of both the fast cross-luminescence and self-trapped exciton (STE) emission. Figure based on van Eijk (1994). (b) The emission spectra recorded from oxygen-free BaF$_2$ crystals at 300 K under excitation by 90 eV photons. The blue solid line depicts the fast cross-luminescence with a decay time of about 600 ps, extending from the deep-UV to UV (<280 nm), which was recorded in a time window (TW) of duration 3.5 ns. The dotted yellow line shows the time-integrated (TI) luminescence signal of the slow STE emission peaked near 300 nm with a decay time of approximately 800 ns. For details of the time-resolved measurements refer to Kirm *et al* (2002).

Table 1. Overview of the general characteristics of BaF$_2$, LSO:Ce and BGO. Values are taken from Lecoq *et al* (2017) unless otherwise indicated.

Property	BaF2	LSO:Ce	BGO
Density ρ (g cm^{-3})	4.88	7.4	7.13
Effective atomic number, Z_{eff}	53	66	75.2
Photon absorption α @511 KeV (cm^{-1})	0.085	0.28	0.336
Radiation length X_0 (cm)	2	1.1	1.12
Intrinsic light yield, LY_{intr} (ph/MeV)	1400[a b h]–7000[b i]	40 000[b]	10 000[b]
Decay time τ (ns)	0.6–0.8[h]/620[i]	22/44[b]	46/365[b]
Photon fraction @ 0.5 MeV	0.19[c])	0.34[c]	0.43[c]
Emission peak(s) λ_{max} (nm)	195[i] 220[i] 310[h]	420[b]	480[b]
Refractive index (RI) @λ_{max}	1.56[d]1.55[d] 1.50[d]	1.82[b]	2.1[b]
Melting point (°C)	1280[e]	2150[f]	1050[f]
Cost ($ cm^{-3})	15[g]	60[g]	35[g]

[a] Dorenbos *et al* 1992.

[b] Gundacker *et al* 2020.

[c] Derenzo 2008.

[d] Malitson 1964, Li 1980.

[e] Zhu 2015.

[f] Sarukura *et al* 2015.

[g] Bell 2012.

[h] Cross-luminescence.

[i] Self-trapped-excition emission.

challenge for photodetectors, as the generated light is emitted in the deep-UV, i.e. peaked at 195 nm and 220 nm (see figure 1) and extending down to 170 nm at 300 K (Kirm *et al* 2002).

Lutetium-based scintillators, for example cerium-doped lutetium–yttrium oxyorthosilicate (LYSO:Ce) or lutetium orthosilicate (LSO), are the workhorses of time-of-flight PET (TOF-PET) but are still relatively expensive, whereas BaF$_2$ crystals are rather cheap to produce. They even cost less to produce than bismuth germanate (BGO), which is a popular cheap scintillator. According to the Handbook of Particle Detection and Imaging (Bell 2012), the price of 1 cm^3 of LSO is about $60, of BGO about $35 and of BaF$_2$ only about $15, which is approaching the price of a fast plastic scintillator (about $11). The low production cost of BaF$_2$ crystals is due to their modest raw material cost and the relatively low temperature at which the crystals are grown. A comparative overview of these three scintillators can be found in table 1.

The discovery in the 1980s of fast cross-luminescence in BaF$_2$, and also in CsF (Laval *et al* 1982, 1983), opened up unmatched possibilities for TOF-PET. Several PET machines that used BaF$_2$ (Lewellen *et al* 1988, Ishii *et al* 1990, Bruyndonckx *et al* 1997) and also CsF (Allemand *et al* 1980, Mullani *et al* 1981, Ter-Pogossian *et al* 1982) were developed. These were the first TOF-PET scanners; they had a reasonable time resolution between 450 ps and 750 ps full width at half maximum (FWHM), a real achievement at the time. However, with the technical limitations in fast electronics it was not possible to make optimal use of the timing potential of the crystal. Furthermore, the use of solar-blind photomultiplier tubes (PMTs) with moderate quantum efficiency and time transfer spread together with the need for high-quality quartz windows reduced the practicality of such systems. In addition, the density of the cross-luminescence materials was too low to compete with the high density of BGO, making the advantages of the available TOF resolution less important than the loss in sensitivity. This was further consolidated by the advances in computational power and the development of fast reconstruction algorithms, solving the Radon transform. In the end, BaF$_2$ and other cross-luminescent materials faded from use in TOF-PET and have never been implemented in large-scale production of PET scanners.

Nowadays, new developments in silicon photomultipliers (SiPMs) have led to good photon detection sensitivity in the deep-UV, making it possible to once more take advantage of the fast cross-luminescence emission in BaF$_2$. This is of special interest because SiPMs, produced in well-controlled complementary metal–oxide–semiconductor processes, have the potential to be extremely cheap. They are robust and insensitive to magnetic fields, making multimodal systems like PET combined with magnetic resonance imaging (MRI) possible. PET/MRI systems in particular ought to greatly benefit from ultrafast timing, as the attenuation sinogram can be determined by TOF only (Defrise *et al* 2012). Furthermore, by doping BaF$_2$ with cadmium (Nepomnyashchikh *et al* 2005), yttrium (Chen *et al* 2018) or lanthanum (Rodnyi *et al* 1991) the slow self-trapped exciton (STE) emission can be almost completely suppressed. This crystal engineering can play an important role in high-rate PET, for example in-beam dose monitoring in hadron therapy, and in HEP experiments with high-luminosity colliders, where the crystal response has to be fast in order to minimize pile-up effects. A possibly even more exciting application of such crystal engineering could be TOF computed tomography (TOF-CT) (Rossignol *et al* 2020), a new technique expected to bring enormous benefits to medical diagnostics.

This paper will discuss the emission timing properties of various BaF$_2$ crystals undoped and doped with cadmium, yttrium and lanthanum. State-of-the-art coincidence time resolution (CTR) measurements with 511 keV gammas will be reported and the timing prospect of BaF$_2$ in PET discussed with regard to the application of new SiPMs that are sensitive in the deep-UV.

2. Materials and methods

2.1. Studied BaF$_2$ samples

Table 2 gives an overview of the samples studied in this work. We used two standard crystals provided by commercial companies, Epic Crystals and Proteus. In order to study the suppression of the slow 800 ns decay component we investigated several crystals with different dopings, produced by the Vinogradov Institute of Geochemistry SB RAS, Irkutsk, and one sample doped with yttrium by Siccas. In previous studies we evaluated the intrinsic light yield of the BaF$_2$ samples from Epic used here and found a value of 8500 photons/MeV (including the STE emission) (Gundacker *et al* 2020). The undoped BaF$_2$ samples from the Vinogradov Institute have a similar intrinsic luminescence of about 9400 photons/MeV (Shendrik and Radzhabov 2014).

All crystals from the Vinogradov Institute, detailed in table 3, were grown by the Stockbarger method with graphite crucibles in vacuum and a growth velocity of about 5 mm h^{-1}. Oxygen-free crystals were grown with the addition of CdF$_2$ as an oxygen scavenger. The concentration of LaF$_3$ impurities varied from 0.01 to 30 mol.%. This was measured using the atomic absorption and emission techniques in Nepomnyashchikh *et al* (2001). Cadmium impurities were added to the raw materials for CdF$_2$ crystal growth in amounts of 0.01 to 2 wt%. High-purity alkaline earth fluoride powders or 'melted' raw materials (better than 99.99%) were used. The crystals were grown in vacuum using a graphite crucible that was closed by a lid to prevent evaporation of CdF$_2$ (Radzhabov *et al* 2005). The achieved concentration of cadmium impurities in the crystals was several times lower than that added to the melt.

The x-ray luminescence spectra of these samples are shown in figure 2(a). These were measured using an x-ray tube with a Pd anode operating at a voltage of 50 kV voltage and a current of 1 mA. The spectra were recorded in the photon-counting regime using a VM-4 vacuum monochromator (Novosibirsk) and an FEU-39A photomultiplier, equipped with a quartz window. All spectra were corrected for the wavelength-dependent sensitivity of the detection system. The luminescence spectra were recorded in the same conditions and geometry for a comparison of relative light output. Figure 2(b) shows that La doping basically does not change the core valence luminescence in the range of 185 nm to 250 nm up to a concentration of about 10 mol.%, with a drop in light yield at higher La concentrations.
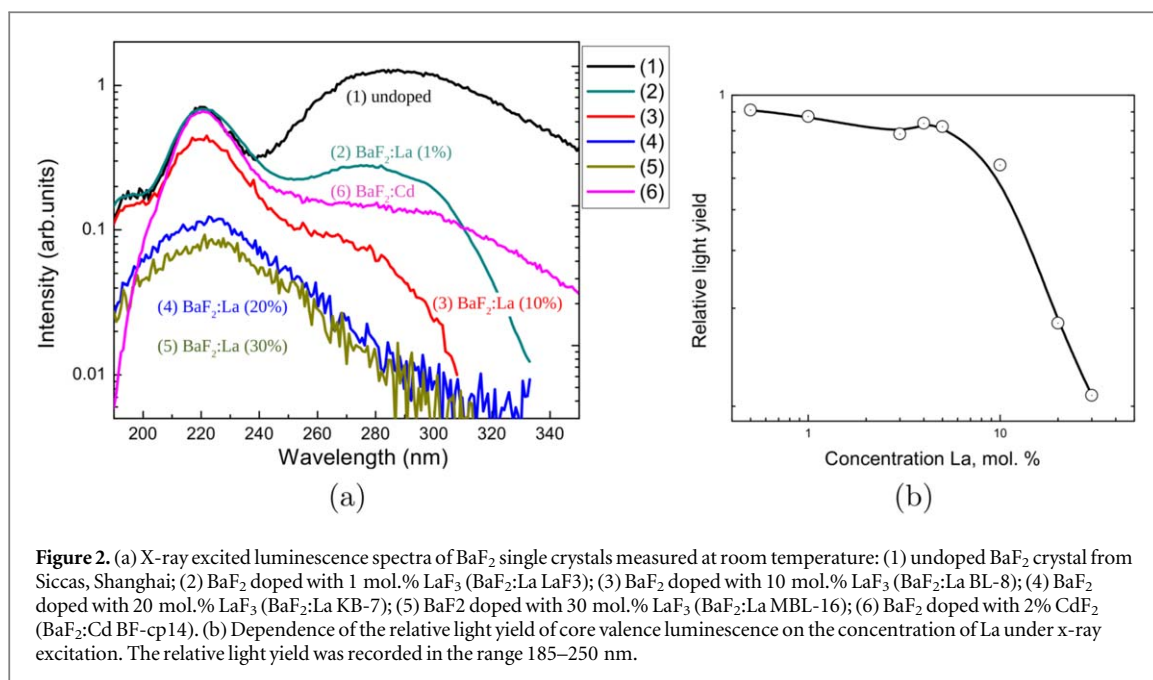
Figure 2. (a) X-ray excited luminescence spectra of BaF_2 single crystals measured at room temperature: (1) undoped BaF_2 crystal from Siccas, Shanghai; (2) BaF_2 doped with 1 mol.% LaF_3 (BaF_2:La LaF3); (3) BaF_2 doped with 10 mol.% LaF_3 (BaF_2:La BL-8); (4) BaF_2 doped with 20 mol.% LaF_3 (BaF_2:La KB-7); (5) BaF2 doped with 30 mol.% LaF_3 (BaF_2:La MBL-16); (6) BaF_2 doped with 2% CdF_2 (BaF_2:Cd BF-cp14). (b) Dependence of the relative light yield of core valence luminescence on the concentration of La under x-ray excitation. The relative light yield was recorded in the range 185–250 nm.

Table 2. Overview of the different BaF_2 scintillators studied in this work.

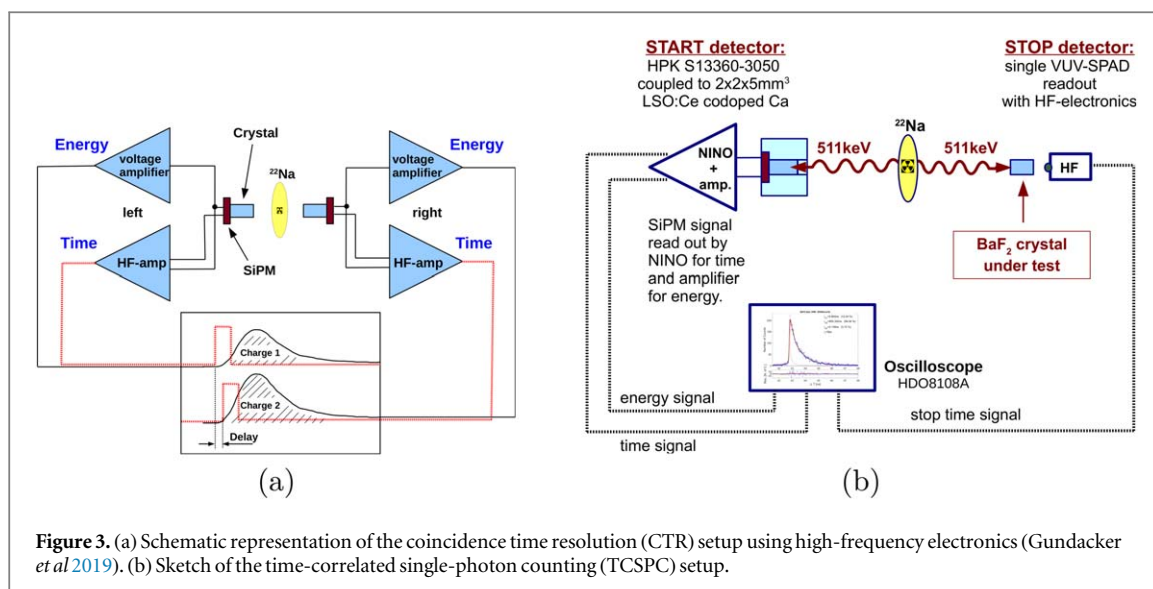| Composition	Producer	Doping
BaF_2	Epic Crystals	—
BaF_2	Proteus	—
BaF_2:CdF_2	Vinogradov Institute	Cadmium difluoride
BaF_2:LaF_3 (5 types)	Vinogradov Institute	Lanthanum trifluoride
BaF_2:Y	Siccas	Yttrium (3 mol.%)

Table 3. Overview of the doped BaF_2 samples from the Vinogradov Institute studied in this work.

Sample pseudonym	Full name
BaF_2:La BaL-12-1	BaF_2 doped with 0.1 mol.% LaF_3
BaF_2:La LaF3	BaF_2 doped with 1 mol.% LaF_3
BaF_2:La BL-8	BaF_2 doped with 10 mol.% LaF_3
BaF_2:La KB-7	BaF_2 doped with 20 mol.% LaF_3
BaF_2:La MBL-16	BaF_2 doped with 30 mol.% LaF_3
BaF_2:Cd BF-cp14	BaF_2 doped with 2% CdF_2

Further information on these samples can be found in the following works: characterization of radiation induced defects of sample BL-8 was performed in Radzhabov *et al* (1998); thermally stimulated luminescence and excitation were studied in Nepomnyashchikh *et al* (2002); excitation spectra under synchrotron excitation were investigated and published in Radzhabov *et al* (2006, 2007) for La-doped samples and Radzhabov and Kirm (2005) and Radzhabov *et al* (2006) for Cd-doped samples.

2.2. Vacuum ultraviolet-sensitive SiPMs

Vacuum ultraviolet high-density (VUV-HD) SiPMs, usable for the detection of cross-luminescence emission in BaF_2, were initially developed by Fondazione Bruno Kessler (FBK) (Gola *et al* 2019) and Hamamatsu Photonics K.K. (HPK) for the search for dark matter and neutrinoless double beta decay. In a previous publication (Pots *et al* 2020) we studied devices from HPK; in the current paper we focus on SiPMs produced by FBK. The FBK devices have an active area of 2.63 mm × 2.90 mm with a single-photon avalanche diode (SPAD) pitch of

Figure 3. (a) Schematic representation of the coincidence time resolution (CTR) setup using high-frequency electronics (Gundacker *et al* 2019). (b) Sketch of the time-correlated single-photon counting (TCSPC) setup.

35 μm. The photon detection efficiency (PDE) is reported to be ~22% at 175 nm (Gola *et al* 2019) and at 410 nm we measured the PDE to reach values of 58%. The intrinsic single-photon time resolution (SPTR) was measured to be 72 ps FWHM at 420 nm, illuminating the entire active area of 2.63 mm × 2.90 mm, after subtracting the electronic noise and laser pulse width following the method described in Gundacker *et al* (2020). The intrinsic SPTR value of the FBK VUV-HD device is very comparable to the FBK near-UV (NUV)-HD device (68 ps FWHM) (Gundacker *et al* 2020). The breakdown voltage was measured to be 33.1 V. All measurements in this paper were performed at 42 V SiPM operation voltage (8.9 V overvoltage) unless stated otherwise. The PDE and SPTR values reported were also measured at 42 V bias voltage.
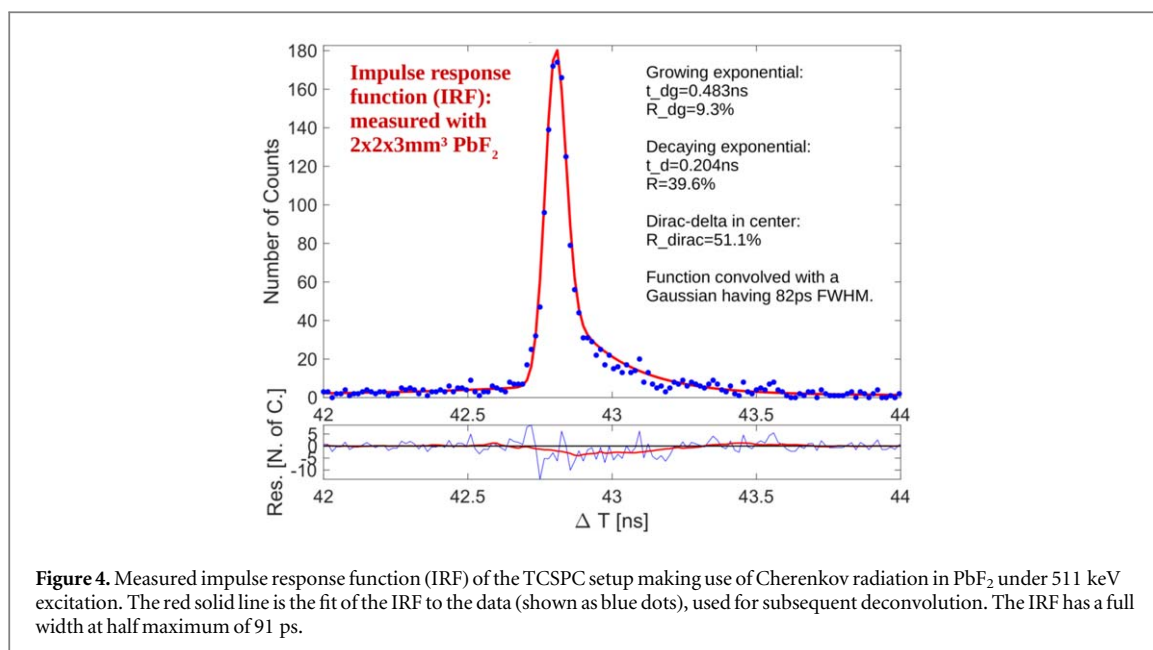
2.3. VUV photoluminescence and 100 keV pulsed cathodoluminescence

The decay kinetics of the doped BaF_2 samples under synchrotron radiation excitation by VUV photons were studied using the photoluminescence endstation of the FinEstBeAMS beamline (Pankratov *et al* 2019) at the MAX IV Laboratory in Lund, Sweden. The 1.5 GeV storage ring was operated in a single bunch mode providing 180 ps FWHM pulses with an interval of 320 ns between subsequent pulses. An intense photon beam was generated by an elliptically polarizing undulator (Pärna *et al* 2017), which, along with the first harmonic used to excite the samples, provides the second harmonic at double energy coinciding with the second-order transmission of the primary monochromator. Therefore, a special effort has to be made to suppress higher harmonic radiation while using the primary monochromator in grazing incidence geometry (Vasil'ev *et al* 1985). Sn and Mg thin metal film filters were inserted into the optical path of the beamline for higher-order suppression at 22 eV and 45 eV photon excitation energies, respectively. The luminescence was detected by an R3809U-50 micro-channel plate (MCP)-PMT mounted together with a filter holder directly on the quartz window of the sample chamber. A lowest occupied molecular orbital narrow-band interference filter was used to select the 216 nm emission, which is due to cross-luminescence in BaF_2. The MCP-PMT signal was processed by an 1 GHz ORTEC 9327 timing discriminator and time stamped by a Chronologic xTDC4 time-to-digital converter, synchronized with the storage ring master frequency using a bunch-clock. An undoped high-quality BaF_2 crystal was also investigated as an intentionally dopant-free reference. This crystal was grown at the St Petersburg State Optical Institute (GOI). All studies were performed at $T = 297$ K.

The pulsed cathodoluminescence (PCL) decay kinetics were recorded for the BaF_2 crystals doped with La or Cd ions using the PCL setup discussed in detail in Omelkov *et al* (2018). The samples grown at the Vinogradov Institute were cut from the boules and ground to size (about 7 mm × 7 mm × 3 mm), but the surfaces exposed were not polished. As a reference, a pure BaF_2 powder sample (99.999%) from Sigma-Aldrich was used. The excitation electron pulses (250 ps FWHM) had a maximum energy of ~110 keV and peak current density of ~16 A cm^{-2}. All decay curves were recorded at $T = 297$ K.

2.4. Coincidence time resolution

The CTR was measured with the standard setup explained in Gundacker *et al* (2013); a schematic representation can be seen in figure 3(a). A ^{22}Na source emits two 511 keV gammas which are detected in coincidence. At one side of the coincidence setup we mounted a reference detector, i.e. a LSO:Ce:Ca crystal of size 2 mm × 2 mm × 3 mm coupled to an FBK NUV-HD SiPM and, on the other side, the BaF_2 crystal under test, a 2 mm × 2 mm × 3 mm

Figure 4. Measured impulse response function (IRF) of the TCSPC setup making use of Cherenkov radiation in PbF$_2$ under 511 keV excitation. The red solid line is the fit of the IRF to the data (shown as blue dots), used for subsequent deconvolution. The IRF has a full width at half maximum of 91 ps.

crystal coupled to an FBK VUV-HD SiPM. The technologies of the VUV-HD SiPM for CTR measurements and the SPAD for the time-correlated single-photon counting (TCSPC) measurements are similar, especially considering the detection efficiency as a function of the wavelength. The front-end to read the SiPM signal employs a small radio-frequency (RF) Balun transformer monitoring the voltage drop between the SiPM anode and cathode. The differential readout circuit was described in Cates *et al* (2018) and is able to read the fast voltage drop across the SiPM without significant bandwidth limitation, allowing for a very fast SiPM single-cell signal rise time (significantly less than 1 ns). The front-end was modified to additionally read, with low amplification, the signal at the SiPM anode. The amplification of this 'energy' signal is unity and can be used to monitor the energy deposited in the SiPM coupled scintillator via charge integration or via the voltage amplitude. A more in-depth discussion on the readout electronics can be found in Gundacker *et al* (2019).

The electronic signals were digitized by a LeCroy DDA735Zi oscilloscope with a bandwidth of 3.5 GHz and a sampling rate of 40 gigasamples (Gs) s^{-1} (using four channels this reduces to 20 Gs s^{-1}, i.e. 50 ps binning). The leading edge threshold was set on the oscilloscope calculating the signal crossing time via linear interpolation. The measured CTR was corrected for the reference detector (LSO:Ce:Ca crystal 2 mm $\times$ 2 mm $\times$ 3 mm coupled to the FBK NUV-HD SiPM) timing of 58 ps FWHM (Gundacker *et al* 2019), allowing us to state the CTR as if two BaF$_2$ crystals were measured in coincidence.

2.5. Time-correlated single-photon counting with 511 keV gamma excitation

The scintillation emission kinetics of the studied scintillators were measured with a TCSPC setup using 511 keV gamma excitation, as shown in figure 3(b). A ^{22}Na source was placed in the middle of a coincidence setup, with one side being a reference start detector and the other side the BaF$_2$ crystal. A complete description of the setup can be found in Gundacker *et al* (2016) and Gundacker *et al* (2018). As the start detector we used a 2 mm $\times$ 2 mm $\times$ 5 mm LSO:Ce:0.4%Ca crystal wrapped in Teflon and coupled to an HPK S13360-3050 SiPM with Meltmount and read out with the NINO front-end electronics (Gundacker *et al* 2013). As the stop detector we used a single VUV-SPAD from FBK adapted to the emission of BaF$_2$ at 200 nm. The VUV-SPAD was placed about 2 mm in front of the 2 mm $\times$ 2 mm surface of the BaF$_2$ crystal, which was unwrapped and placed on top of a black crystal holder. This arrangement allowed a low probability of detecting scintillation photons, which ensured ongoing measurements to be in single-photon counting mode. The VUV-SPAD was read out by the high-frequency electronics discussed in Gundacker *et al* (2019). We used a LeCroy HDO8108A to digitize the waveforms, selecting only photoelectric events in the start detector but accepting all events regardless of the energy deposition in the crystal under test (BaF$_2$). The data were analyzed offline in Matlab.

The measured scintillation time profile is a convolution of the real BaF$_2$ scintillation emission with the impulse response function (IRF) of the setup. In order to calibrate and to determine the exact IRF we used prompt Cherenkov emission in a PbF$_2$ crystal of the same dimension as the tested BaF$_2$. This takes not only the timing contribution of the start, stop detectors and oscilloscope into account, but also the photon transfer time spread (PTS) of the scintillation light in the crystal itself. This method has been described in Gundacker *et al* (2016). The
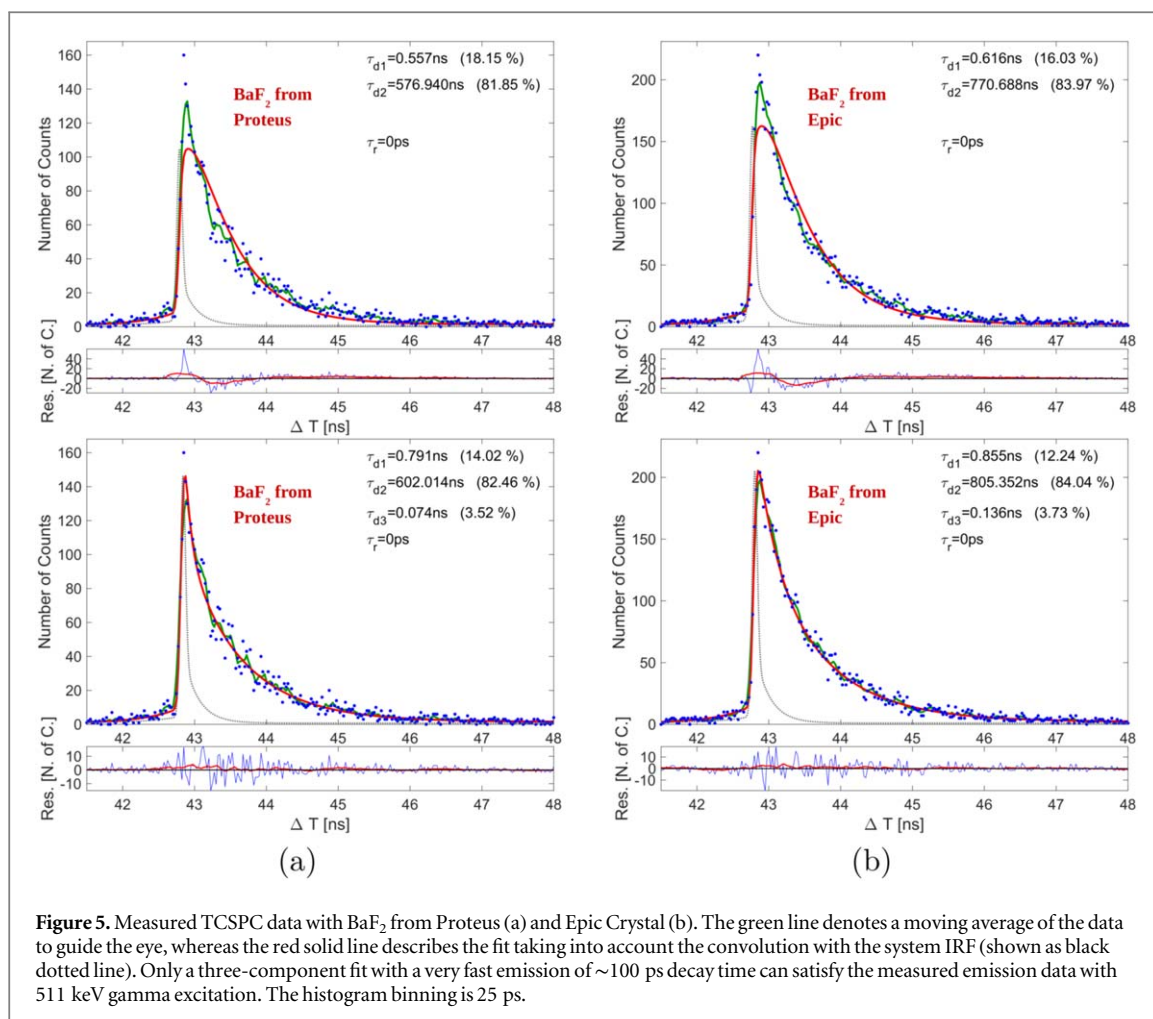
Figure 5. Measured TCSPC data with BaF_2 from Proteus (a) and Epic Crystal (b). The green line denotes a moving average of the data to guide the eye, whereas the red solid line describes the fit taking into account the convolution with the system IRF (shown as black dotted line). Only a three-component fit with a very fast emission of $\sim$100 ps decay time can satisfy the measured emission data with 511 keV gamma excitation. The histogram binning is 25 ps.

resulting IRF can be seen in figure 4 with a FWHM of 91 ps. Tails are noticeable; these are caused by diffusion tails of the SPAD, the scintillation PTS in the crystal and some artifacts in the data aquistion of the oscilloscope. It should be noted that by measuring the IRF with Cherenkov emission in PbF_2 such contributions are correctly taken into account in the fit by deconvolving the IRF from the measured scintillation time profile. The fit procedure, applying a double or triple exponential decay, is described in more detail in Gundacker *et al* (2018).

3. Results

3.1. Ultrafast emission in BaF_2 with 511 keV gamma excitation

To study cross-luminescence and the suitability of VUV-SiPMs, we first measured the scintillation kinetics of samples from Epic Crystal and Proteus under 511 keV excitation in our TCSPC setup (Gundacker *et al* 2018) using a VUV-SPAD from FBK as a single-photon detector. Results can be seen in figure 5. Applying a two-component decay fit, one for the cross-luminescence and the other for the STE emission, as commonly suggested in the literature, did not lead to a satisfactory fit for the very start of the scintillation emission. This can be seen in the top plots of figure 5. In order to describe the data correctly we have to include a very fast decay component (Derenzo *et al* 2000, Gundacker *et al* 2020, Pots *et al* 2020) of 74 ps having 3.5% of the total light yield for BaF_2 from Proteus and a decay time of 136 ps having 3.7% of the total light yield for the Epic Crystal sample, as can be seen in figures 5(a) and (b), respectively. The other decay components are 791 ps (14.0%) and 602 ns (82.5%) for Proteus and 855 ps (12.2%) and 805 ns (84.0%) for Epic Crystal. We further evaluated the rise time with our fit routine and constantly found rise time values of less than 4 ps, far below the resolution of our system, given by the IRF of 91 ps FWHM. In fact such small rise times can be considered equal to 0 ps for applications in PET. Hence, in order to estimate the decay times with higher precision, especially in view of the ultrafast emission, the presented fit values were derived by setting the rise times in the fit to zero, which is justified by the previously obtained results.

Table 4. Scintillation rise and decay times measured for BaF_2 crystals from the producer Epic Crystal (Ep.) and Proteus (Pr.). Two exponential decay fits are compared with three exponential decay fits and when the crystals are wrapped in Teflon (Tef.) or left unwrapped. Errors are given in $\pm 1\sigma$, meaning a confidence interval of 68%.

Origin	τ_r (ps)	τ_{d1} (ns)	R_1 (%)	τ_{d2} (ns)	R_2 (%)	τ_{d3} (ns)	R_3 (%)	τ_{deff} (ns)[a]
Ep. Tef.	<4	0.207 ± 0.087	3.0 ± 1	0.842 ± 0.059	10.6 ± 1.1	692 ± 28	86.4 ± 0.7	3.676
Ep.	<4	0.136 ± 0.052	3.7 ± 0.7	0.855 ± 0.055	12.2 ± 1.0	805 ± 56	84.0 ± 1.1	2.405
Pr. Tef.	<4	0.118 ± 0.050	2.0 ± 0.5	0.814 ± 0.040	9.1 ± 0.5	648 ± 21	88.9 ± 0.7	3.538
Pr.	<4	0.074 ± 0.035	3.5 ± 0.7	0.791 ± 0.034	14.0 ± 1.1	602 ± 48	82.5 ± 1.4	1.535
Ep. Tef.	<4	—	—	0.656 ± 0.011	13.6 ± 0.6	678 ± 27	86.4 ± 0.6	4.794
Ep.	<4	—	—	0.616 ± 0.021	16.0 ± 1.0	771 ± 53	84.0 ± 1.0	3.834
Pr. Tef.	<4	—	—	0.639 ± 0.018	10.9 ± 0.4	637 ± 21	89.1 ± 0.4	5.815
Pr.	<4	—	—	0.557 ± 0.020	18.1 ± 1.0	577 ± 48	81.9 ± 1.3	3.064

[a] $\tau_{deff} = (R_1/\tau_{d1} + R_2/\tau_{d2} + R_3/\tau_{d3})^{-1}$.

It is interesting to notice that previous work by Derenzo *et al* (2000) observed a similar ultrafast component in BaF_2 with pulsed 30 keV x-ray excitation, read out by a fast MCP-PMT. This was confirmed by x-ray measurements with 40 keV maximum energy and hybrid-PMT readout (Gundacker *et al* 2020, Pots *et al* 2020), although with the disadvantage of an unoptimized detection efficiency of the hybrid-PMT in the deep-UV. That this ultrafast component now is confirmed with 511 keV excitation most likely excludes excitation density effects as its origin.

In order to increase the measured light output and improve timing and energy resolution, PET applications normally wrap the scintillators in a reflective material, e.g. enhanced specular reflector foil, $BaSO_4$ or Teflon. Teflon in particular is of interest for laboratory measurements because of its ease of use. However, Teflon is believed to become transparent in the deep-UV. In order to test the usability of Teflon wrapping for our laboratory tests we measured the scintillation kinetics of the two BaF_2 samples from Epic Crystal and Proteus when wrapped in at least five layers of Teflon tape. We observed a slight loss of the fast deep-UV light, which lowers the relative intensities of these components, i.e. we measured decay times of 207 ps (3.0% relative light yield), 842 ps (10.6%) and 692 ns (86.4%) for the Epic Crystal sample and 118 ps (2.0% relative light yield), 814 ps (9.1%) and 648 ns (88.9%) for Proteus. The deconvolved scintillation parameters are summarized in table 4, and also give an overview of the measured data when a double exponential fit is applied.

Looking at the fit parameters for the fast emission of BaF_2 in table 4, a clear reduction in relative light intensity of the fast components can be seen if the crystal is wrapped in Teflon. Also, the decay time of the fast components increases, which is directly related to a higher PTS in the scintillator by multiple reflections due to the Teflon wrapping (Gundacker *et al* 2014). Interestingly, crystals from Proteus suffer to a greater extend from Teflon wrapping than those from Epic Crystal, leading to a better CTR performance of crystals from Epic Crystal, especially after Teflon wrapping. This behavior can most likely be explained by a better transparency in the deep-UV seen in crystals from Epic Crystal (Pots *et al* 2020).

3.2. Suppressing the slow emission in BaF_2 with 511 keV gamma excitation

The STE emission in BaF_2 with a decay time of several hundred nanoseconds potentially makes this crystal less attractive for applications that need short recovery times and high event rates. For example, bunch crossing in the Large Hadron Collider at CERN with its 25 ns duration would constitute a major challenge for standard BaF_2, especially in the case of high-luminosity upgrades. Another potential application for BaF_2 could be in-beam dose monitoring for hadron therapy via positron production and TOF-PET techniques, due to the promise of BaF_2 to deliver excellent time resolution. Nevertheless, in-beam dose monitoring in hadron therapy suffers from a huge background of prompt photon emission, which might become manageable if the detector used has a very fast response time. Another application in need of high-rate scintillator-based detectors is single x-ray TOF-CT (Rossignol *et al* 2020) and hard x-ray imagers (Hu *et al* 2019).

For all of these applications the STE emission has to be suppressed in order to reduce pile-up effects. The STE emission peaks very close to the cross-luminescence, and hence it is difficult to suppress the STE emission by means of optical filters alone. However, it has been shown that the slow STE emission in BaF_2 can be sufficiently eliminated by introducing proper doping (Rodnyi *et al* 1991, Hu *et al* 2020). We tested six crystals in view of their emission timing characteristics with 511 keV excitation and different dopings (samples were produced by the Vinogradov Institute and Siccas). The results are reported in table 5 and a graphic representation of all measured STE and cross-luminescence decay times with their relative intensities can be seen in figure 6 for undoped and doped BaF_2 crystals of various origins.
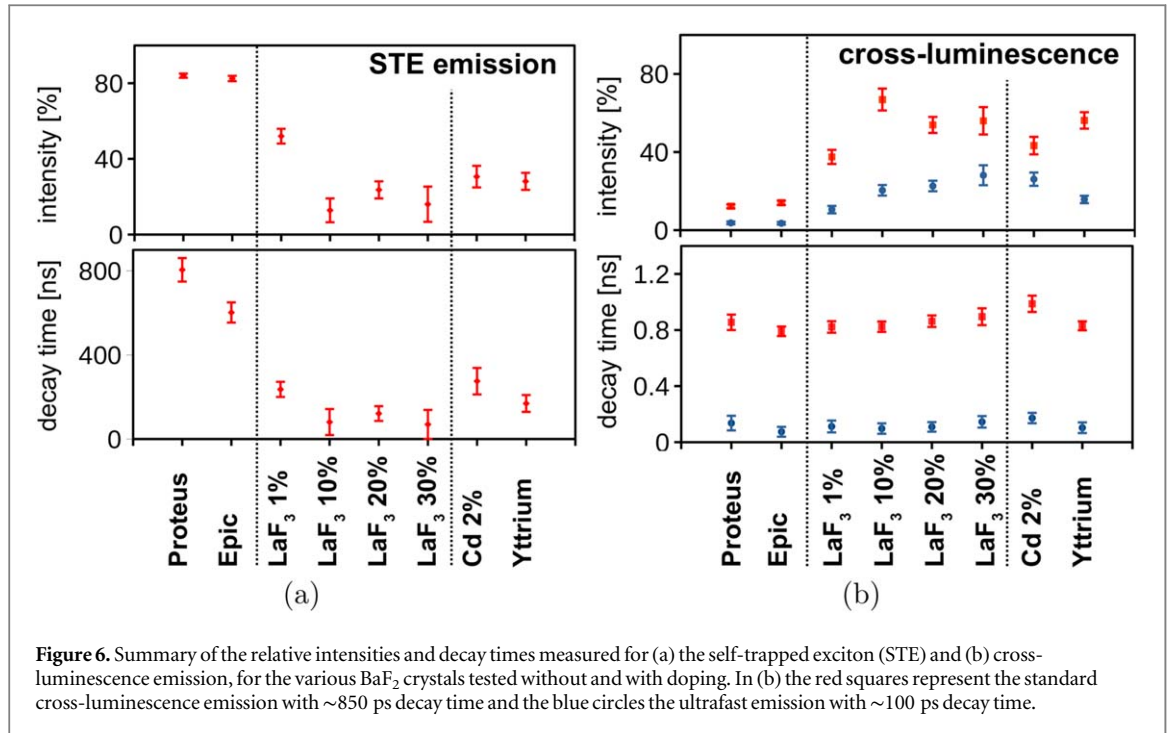
Figure 6. Summary of the relative intensities and decay times measured for (a) the self-trapped exciton (STE) and (b) cross-luminescence emission, for the various BaF$_2$ crystals tested without and with doping. In (b) the red squares represent the standard cross-luminescence emission with ~850 ps decay time and the blue circles the ultrafast emission with ~100 ps decay time.

Table 5. The scintillation time characteristics of BaF$_2$ compared for samples with different doping, suppressing the slowest decay time component (τ_{d3}). Every doping tested successfully suppresses the slow 800 ns STE emission. Errors are given in $\pm 1\sigma$, meaning a confidence interval of 68%.

Doping	τ_r (ps)	τ_{d1} (ns)	R_1 (%)	τ_{d2} (ns)	R_2 (%)	τ_{d3} (ns)	R_3 (%)	$\frac{R_1}{R_1 + R_2}$ (%)
Cd 2%	<4	0.172 ± 0.037	26.1 ± 3.4	0.987 ± 0.058	43.3 ± 4.5	275 ± 63	30.6 ± 5.7	37.6
La 1%	<4	0.112 ± 0.042	10.5 ± 1.9	0.822 ± 0.041	37.5 ± 3.6	236 ± 36	52.0 ± 3.9	21.9
La 10%	<4	0.097 ± 0.037	20.4 ± 2.7	0.824 ± 0.037	66.9 ± 5.6	81 ± 62	12.8 ± 6.3	23.3
La 20%	<4	0.109 ± 0.034	22.6 ± 2.7	0.863 ± 0.041	53.9 ± 4.1	121 ± 35	23.6 ± 4.5	29.5
La 30%	<4	0.145 ± 0.041	28.1 ± 5.1	0.895 ± 0.060	56.0 ± 7.0	69 ± 69	16.0 ± 9.3	33.4
Y	<4	0.103 ± 0.038	15.7 ± 1.9	0.830 ± 0.032	56.2 ± 4.2	169 ± 40	28.1 ± 4.5	21.8

For example, for BaF$_2$ doped with LaF$_3$ we measured for sample BaF$_2$:La 10% (BL-8) decay components of 97 ps with 20.4%, 824 ps with 66.9% and 81 ns with 12.8% relative light yield, as can be seen in figure 7(a) and table 5. In figure 7(b) similar fits with a BaF$_2$ sample from Epic Crystal are shown for comparison. Other decay time measurements performed with BaF$_2$:Cd 2% (BF-cp14) and BaF$_2$:La 30% (MBL-16) can be seen in figure 8. Doping with lanthanum and cadmium clearly suppress the slow 800 ns component to a minimum, with almost no light remaining from this scintillation channel.

Further, LaF$_3$ doping leaves the fast and ultrafast emission of BaF$_2$ to a large extent unchanged, especially for doping concentrations below 10 mol.%, with the same light yield ratio between the ultrafast and fast decay components remaining. Increasing the La concentration, the ultrafast component seems to gain in relative abundance compared with the 'standard' cross-luminescence emission, seen by the ratio $R_1/(R_1 + R_2)$ in table 5. Whilst the reason for this is still under investigation, it can be noted that this behavior is beneficial for maintaining the excellent timing properties of BaF$_2$ doped with La in applications such as PET or HEP, despite a slight reduction in core valence luminescence yield with increasing La concentration, as depicted in figure 2(b). We also want to mention that the slow STE fit parameters (τ_{d3} and R_3) in table 5 for La dopings of 10 mol.% and higher show a greater uncertainty and are only indicative because their recorded intensity is very low, close to the noise floor. To summarize, we can conclude that doping of BaF$_2$ preserves the excellent timing characteristics of cross-luminescence in BaF$_2$, which will be further be discussed in section 3.4.

In Pots *et al* (2020) several TCSPC measurements under x-ray excitation of BaF$_2$ samples from Proteus and Epic Crystal have been performed, placing different filters between the BaF$_2$ crystal and the single-photon detector, a Becker & Hickl hybrid-PMT. It was found that by placing a high-pass filter of 400 nm (cutting all wavelengths larger than 400 nm) no scintillation emission was recorded. Hence, the authors concluded that the
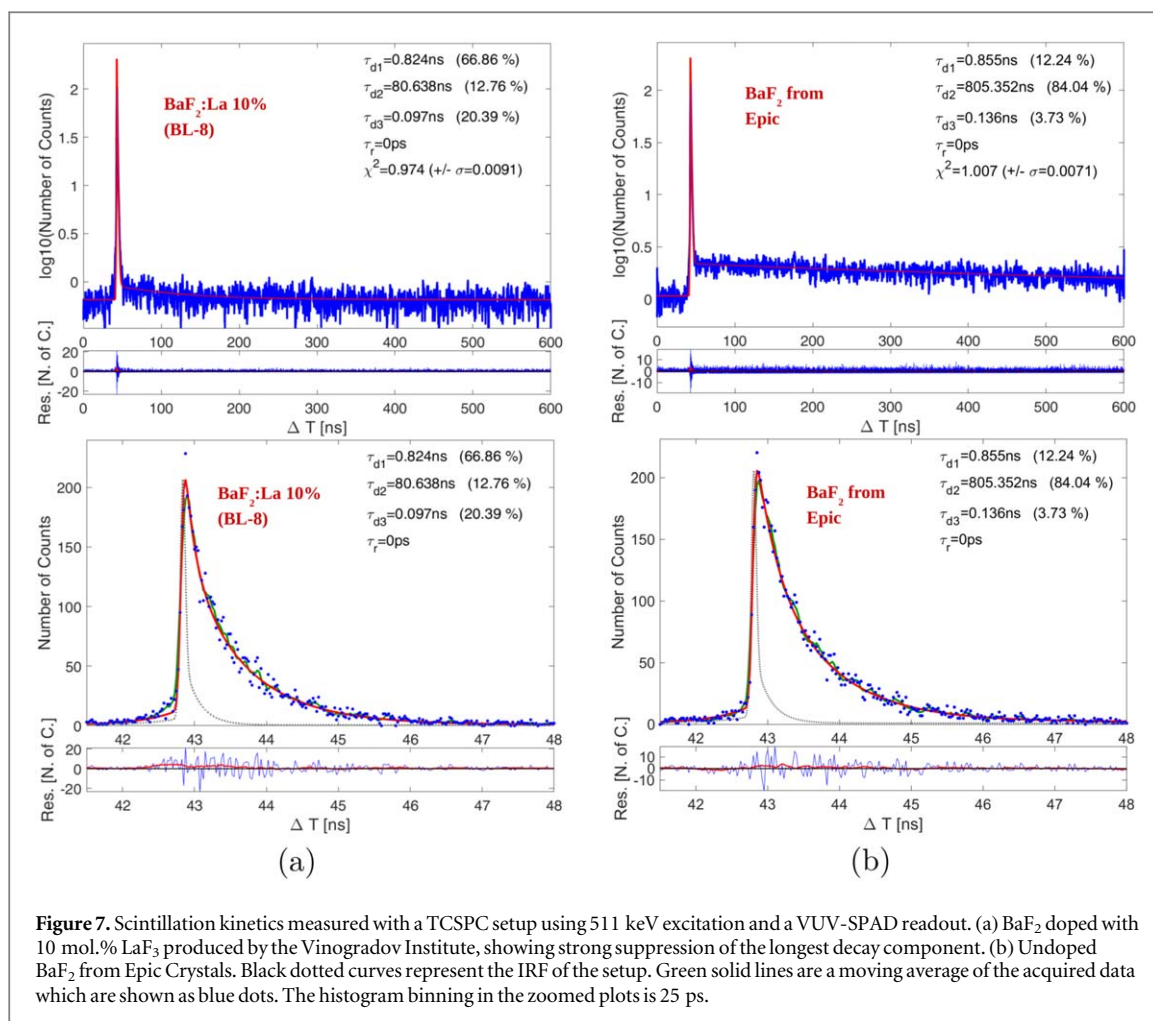
Figure 7. Scintillation kinetics measured with a TCSPC setup using 511 keV excitation and a VUV-SPAD readout. (a) BaF_2 doped with 10 mol.% LaF_3 produced by the Vinogradov Institute, showing strong suppression of the longest decay component. (b) Undoped BaF_2 from Epic Crystals. Black dotted curves represent the IRF of the setup. Green solid lines are a moving average of the acquired data which are shown as blue dots. The histogram binning in the zoomed plots is 25 ps.
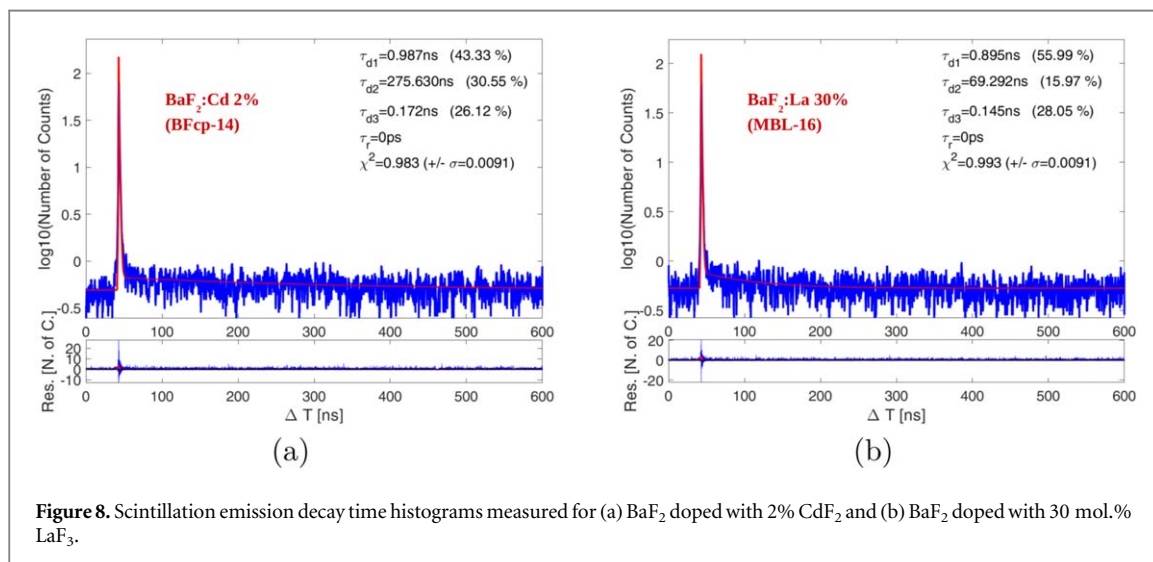

Figure 8. Scintillation emission decay time histograms measured for (a) BaF_2 doped with 2% CdF_2 and (b) BaF_2 doped with 30 mol.% LaF_3.

ultrafast 100 ps emission does not originate from hot-intraband luminescence. The results observed in this work, showing that doping of BaF_2 leaves the fast and ultrafast emission untouched, further confirms the observations in Pots *et al* (2020).

3.3. Results obtained with 110 keV electron and VUV synchrotron radiation excitation

Figure 9 depicts the PCL decay kinetics of BaF_2 doped with La and Cd at various concentrations. As revealed by the results of decay analysis (upper part of table 6) one can see that the decomposition of cross-luminescence
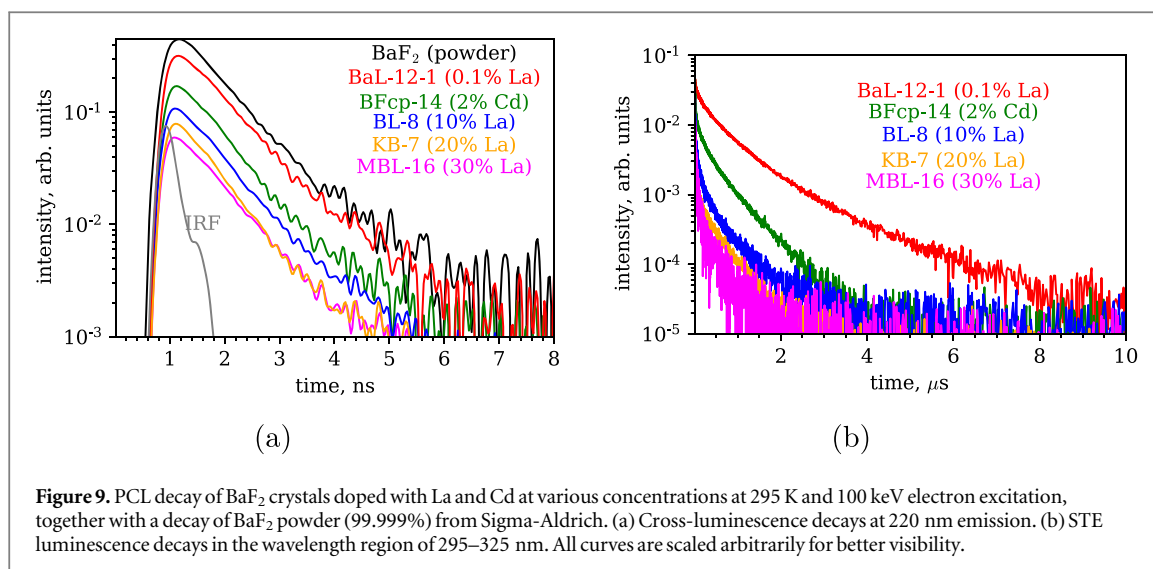
Figure 9. PCL decay of BaF$_2$ crystals doped with La and Cd at various concentrations at 295 K and 100 keV electron excitation, together with a decay of BaF$_2$ powder (99.999%) from Sigma-Aldrich. (a) Cross-luminescence decays at 220 nm emission. (b) STE luminescence decays in the wavelength region of 295–325 nm. All curves are scaled arbitrarily for better visibility.

Table 6. The deconvolution of decay curves of cross-luminescence (220 nm for PCL and 216 nm for VUV photoluminescence) from pure and doped BaF$_2$ samples at 295 K.

Origin	Type	τ_{d1} (ns)	R_1 (%)	τ_{d2} (ns)	R_2 (%)	τ_{d3} (ns)	R_3 (%)
		PCL					
Sigma-Aldrich	BaF$_2$ powder	0.01	5	0.77	95	—	—
Vinogradov Inst.	BaF$_2$:La 0.1%	—	—	0.71	100	—	—
Vinogradov Inst.	BaF$_2$:Cd 2%	0.11	3	0.65	97	—	—
Vinogradov Inst.	BaF$_2$:La 10%	0.06	6	0.67	94	—	—
Vinogradov Inst.	BaF$_2$:La 20%	0.16	7	0.61	93	—	—
Vinogradov Inst.	BaF$_2$:La 30%	0.05	6	0.68	94	—	—
		VUV photoluminescence (22 eV)					
GOI	BaF$_2$ crystal	0.03	7	0.45	71	0.95	22
Vinogradov Inst.	BaF$_2$:La 0.1%	<0.01	3	0.53	83	1.6	14
Vinogradov Inst.	BaF$_2$:La 30%	<0.01	4	0.55	78	1.4	18
		VUV photoluminescence (45 eV)					
GOI	BaF$_2$ crystal	0.03	8	0.43	70	1.0	22
Vinogradov Inst.	BaF$_2$:La 0.1%	<0.01	1	0.61	92	1.6	8
Vinogradov Inst.	BaF$_2$:La 30%	<0.01	4	0.62	83	1.8	12

decay curves recorded at 220 nm and their shape does not significantly change with the addition of doping ions. It is known that introducing impurities to alkali earth fluorides reduces the emission of self-trapped excitons in comparison with that in undoped crystals (Radzhabov *et al* 2008). The PCL studies also indicate that doping with La as well as Cd decreases the intensity of slow STE emission and influences the fast cross-luminescence intensity to a smaller extent. Indeed, figure 9 (right panel) indicates clearly the decrease in STE emission decay times and the non-exponential nature of the decay curves, which is a typical characteristic of quenching processes due to STE diffusion to suppression centers (Radzhabov *et al* 2005).

BaF$_2$ cross-luminescence is known to be sensitive to excitation density effects under excitation by VUV and extreme UV photons introduced by surface quenching or energy transfer from the core hole to other electronic excitations (Terekhin *et al* 1995). The observed cross-luminescence decay of all studied samples (see figure 10) under VUV excitation is non-exponential (see analysis results in table 6, bottom part), but not as visible as for STE. The fit of decay curves reveals that the sum of three exponentials, consisting of ultrafast ($\leqslant$0.03 ns), 'regular' (0.5–0.7 ns) and slow (>1 ns) components, is the best model. The ultrafast component, typically below 30 ps, is far below the time resolution of the current experiment and has to be studied separately with better precision, for example using free electron laser radiation (Kirm *et al* 2005) or short pulse x-ray facilities (Turtos *et al* 2019b). The ultrafast processes in scintillators should be studied with the improved time resolution achievable when excited by ~100 fs photon pulses. It is also obvious that the 'regular' decay component is faster (0.4–0.6 ns) than in the case of electron beams (0.6–0.8 ns) and gamma excitations (0.8–1.0 ns). Notably, La doping, even at small concentrations, decreases the strength of excitation density effects, leading to more exponential decay and 'regular' component closer to the high-energy excitation value. Therefore, small
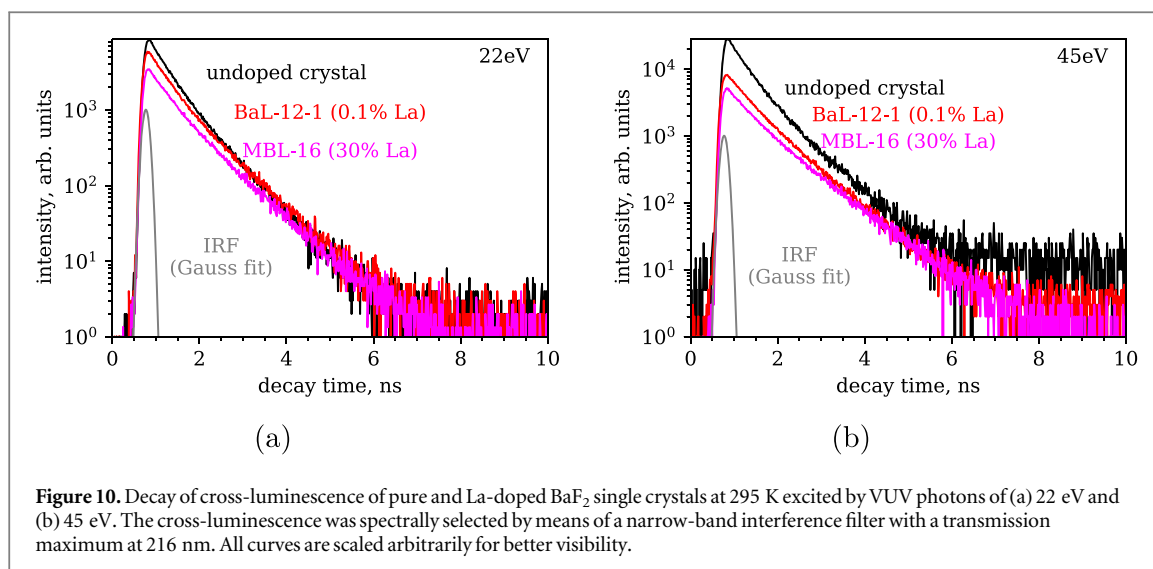
Figure 10. Decay of cross-luminescence of pure and La-doped BaF$_2$ single crystals at 295 K excited by VUV photons of (a) 22 eV and (b) 45 eV. The cross-luminescence was spectrally selected by means of a narrow-band interference filter with a transmission maximum at 216 nm. All curves are scaled arbitrarily for better visibility.

Table 7. The CTR measured for different BaF$_2$ samples with and without doping. The timing properties of the doped samples are comparable to the undoped ones. For comparison an LYSO:Ce sample in the same conditions achieves a much worse CTR, although the PDE of the used VUV-SiPMs at 410 nm is 58% compared with ~22% at 200 nm.

Origin	Type	CTR (ps) (air coupling)
BaF$_2$ from Vinogradov Inst.	BaF$_2$:Cd 2%	73 ± 3 (depolished crystals)
BaF$_2$ from Vinogradov Inst.	BaF$_2$:La 30%	89 ± 3 (depolished crystals)
BaF$_2$ from Proteus	BaF$_2$	68 ± 3
BaF$_2$ from Epic Crystal	BaF$_2$	60 ± 3
BaF$_2$ from Siccas	BaF$_2$	69 ± 3
BaF$_2$ from Siccas	BaF$_2$:Y	62 ± 3
LYSO:Ce from CPI	LYSO:Ce	105 ± 3

concentrations of La might improve other excitation density-dependent scintillation characteristics of BaF$_2$, such as yield non-proportionality with respect to gamma-ray energy (Kamenskikh *et al* 2020) and the response to alpha particles.

3.4. CTR comparison of the various BaF$_2$ samples with air coupling.

With state-of-the-art VUV-HD devices from FBK (Gola *et al* 2019) we measured the CTR of the various BaF$_2$ crystals with and without doping, for which we summarize the results in table 7. For these tests we wrapped the scintillators in Teflon but used no optical coupling agent between the SiPM and crystal (air coupling), in order to ensure that the deep-UV light is not absorbed and transferred to the SiPM. Table 7 underlines that the different samples reach almost the same CTR, measured around 70 ps FWHM. This confirms that doping does not affect the timing performance of BaF$_2$ significantly, for which only the fast cross-luminescence emission and ultrafast component are of importance. Samples from the Vinogradov Institute were depolished on all surfaces, which could have lead to a slightly changed CTR performance (this will be the subject of future studies).

We also measured the CTR of standard LYSO:Ce from CPI in the same conditions with the VUV-HD SiPMs, obtaining a CTR of 105 ps FWHM. The CTR achieved with BaF$_2$ in these tests is remarkable, especially considering that the VUV-SiPM has only about 22% PDE at a wavelength of 200 nm (emission of BaF$_2$) (Gola *et al* 2019) which has to be compared with values of 58% at 410 nm (emission of LYSO:Ce) (Gundacker *et al* 2020). This already hints very clearly at the superb timing properties of BaF$_2$ established by its very fast cross-luminescence, which is confirmed with SiPMs from HPK (Pots *et al* 2020).

3.5. Deterioration of CTR with a lack of optical grease coupling

To investigate the experimental limits of our setup in terms of the best achievable CTR with BaF$_2$ we also conducted studies with different optical glue couplings. In itself glue coupling in the deep-UV is not trivial, even more so when applied in combination with VUV-SiPMs. Since UV light is absorbed very quickly the penetration
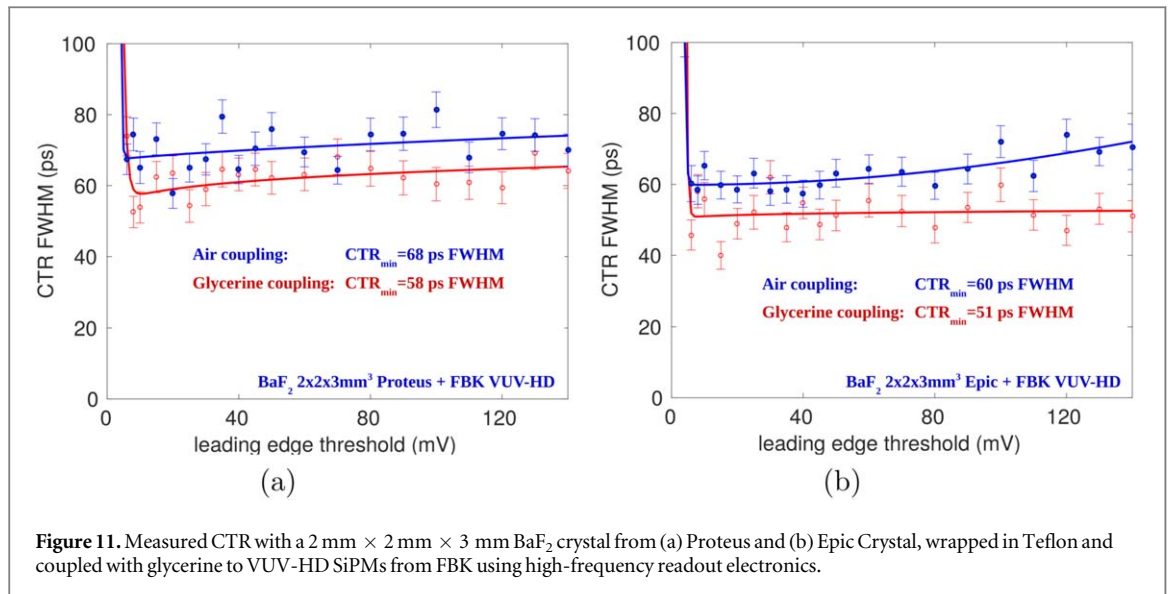
Figure 11. Measured CTR with a 2 mm $\times$ 2 mm $\times$ 3 mm BaF$_2$ crystal from (a) Proteus and (b) Epic Crystal, wrapped in Teflon and coupled with glycerine to VUV-HD SiPMs from FBK using high-frequency readout electronics.

depth is very shallow, for which the SiPM anti-reflective coating (ARC) and SPAD structure have to be adapted. Furthermore this prohibits the use of protective layers on top of the SiPM entrance window, for example glass/ resin coating or sometimes even thin passivation layers. Hence, the applied glue can distort the ARC and even the functionality of the SiPM, which can be seen in an increased dark count rate or a full destruction of the SiPM in certain cases. Following the previous work with HPK SiPMs in Pots *et al* (2020) we tested different coupling agents along with glycerine, which worked for the VUV-HD SiPMs from FBK. We found that the coupling is not straightforward and that older glycerine tends to destroy the SiPM, especially after cleaning with ethanol.

Applying glycerine coupling we measured a CTR of 58 ± 3 ps and 51 ± 3 ps with 2 mm $\times$ 2 mm $\times$ 3 mm BaF$_2$ crystals from Proteus and Epic Crystal, respectively. In both cases the crystals were wrapped in Teflon. In figure 11 we compare these results with the CTR measurements with air coupling, which lead to a CTR of 68 ± 3 ps and 60 ± 3 ps FWHM for Proteus and Epic Crystal samples, respectively. The CTR ratio between grease and air coupling is 1.17, which in quadrature is 1.37, meaning that with glycerine coupling about 37% more of the cross-luminescence light was detected. This is in good agreement with the light transfer efficiency simulations in Gundacker *et al* (2020) and measurements in Pots *et al* (2020). However, it should be noted that for CTR only the extracted light of the fastest components in the deep-UV is of importance and, hence, so is the transparency of the coupling agent and crystal itself to light with a wavelength around 200 nm.
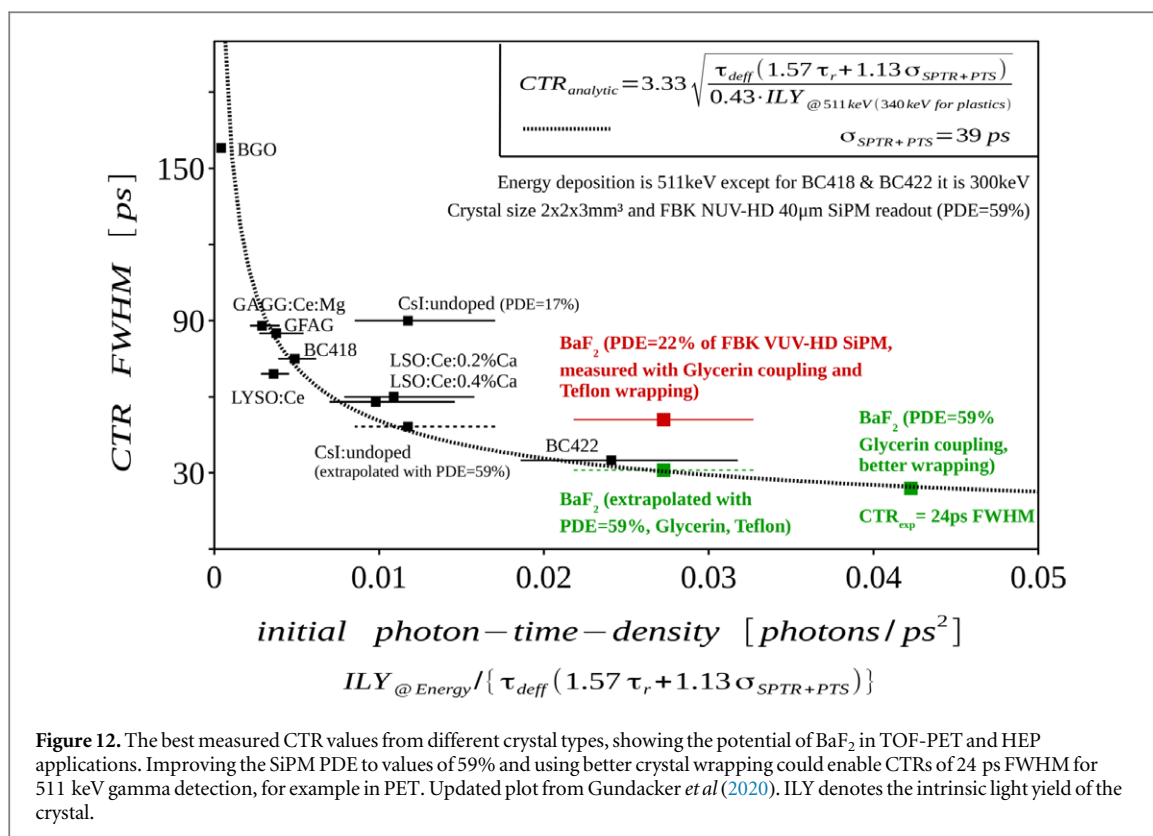
The best CTR result obtained with BaF$_2$ (51 ps FWHM with FBK VUV-HD SiPMs) has to be compared with the experimentally best achieved CTR with LSO:Ce co-doped with 0.4% Ca from Agile (58 ps FWHM) obtained by Gundacker *et al* (2019) using FBK NUV-HD SiPMs. Further a CTR of 69 ps FWHM was achieved with 2 mm $\times$ 2 mm $\times$ 3 mm LYSO:Ce from CPI coupled to NUV-HD SiPMs (Gundacker *et al* 2020). These measurements applied the same readout electronics, crystal geometry and Teflon wrapping and mounted the crystal to the SiPM with transparent optical coupling agents. The only difference is the reported PDE values for both devices, with ~22% (Gola *et al* 2019) at 200 nm for the VUV-HD SiPM and 65% at 410 nm for the NUV-HD SiPM.

This immediately shows the high potential of BaF$_2$ with SiPM readout for ultrafast timing, already beating the state-of-the-art with LSO:Ce:Ca, despite an SiPM PDE that is lower by a factor of 3.

4. Perspectives of BaF$_2$ in TOF-PET

The now moderate PDE performance seen in VUV-SiPMs leaves room for some technological improvements. In order to get an understanding of the potential of BaF$_2$ we compare in figure 12 the timing limits of commonly used inorganic scintillators in TOF-PET and HEP (Gundacker *et al* 2020). The figure uses the scintillation kinetics reported in table 4 for BaF$_2$ from Epic Crystal wrapped in Teflon and also considers the ultrafast sub-100 ps decay component.

If we could optimize the VUV-HD SiPM PDE to boost the 22% value to 59% (achieved with state-of-the-art SiPMs for, e.g., LYSO:Ce readout) a CTR limit of 31 ps FWHM would be in reach according to the analytical model discussed in Vinogradov (2017). Moreover, analyzing the values in table 4 we notice that with better wrapping, having a higher reflectivity in the deep-UV, the CTR could be even further improved to values around 24 ps FWHM. This estimation was performed considering an SPTR of 72 ps FWHM measured for a VUV-SiPM

Figure 12. The best measured CTR values from different crystal types, showing the potential of BaF$_2$ in TOF-PET and HEP applications. Improving the SiPM PDE to values of 59% and using better crystal wrapping could enable CTRs of 24 ps FWHM for 511 keV gamma detection, for example in PET. Updated plot from Gundacker *et al* (2020). ILY denotes the intrinsic light yield of the crystal.

at 420 nm. In view of the ultrafast, almost prompt, emission in BaF$_2$ with decay times below 100 ps, the SPTR gains a special importance, as was shown in Gundacker *et al* (2016). Hence, improving the SPTR of the VUV-SiPM opens an additional route to push the CTR limits with BaF$_2$ even further (Acerbi and Gundacker 2019, Lecoq *et al* 2020).

5. Discussion

The presented studies show that cross-luminescence, for example in BaF$_2$, continues to be a very promising ultrafast emission for achieving the highest time resolution when detecting high-energetic gamma and charged particles. Furthermore, the development of VUV-SiPMs opens up cost-effective readout technology for these crystals, and most likely will push the possibilities and prospects of cross-luminescence for various applications, similar to the introduction of SiPMs in TOF-PET (Gundacker and Heering 2020).

The aim of the current study was to highlight the excellent material properties of BaF$_2$ and several dopants to suppress the slow STE emission. Using 511 keV excitation we confirmed an ultrafast emission with a sub-100 ps lifetime alongside the standard cross-luminescence with 800 ps decay time. This substantiates the results of Derenzo *et al* (2000), who also measured an ultrafast sub-100 ps decay component in BaF$_2$ with 30 keV x-ray excitation. This ultrafast component, with an absolute light yield of about 300 photons/MeV energy deposit, can give a unique handle to achieve unmatched time resolution in TOF-PET. The best CTR measured was 51 ps FWHM, using short crystals of size 2 mm × 2 mm × 3 mm. We have further shown that by improving the VUV-SiPM PDE to values of 59% with additional development of wrapping materials could make CTRs of 24 ps FWHM possible.

The presented measurements with rather short crystals of 3 mm can be seen as a best case scenario, already valid and applicable for system-related aspects in the field of TOF-CT, where even shorter crystals could be used due to the lower x-ray energies of around 100 keV. For TOF-PET applications, on the other hand, solutions to increase detection efficiency have to be found, especially for PET system sensitivity. There are two immediate approaches one could follow. The first could be to increase the amount of material or build bigger scanners. If the promise of BaF$_2$, being substantially cheaper than LYSO, can be fulfilled, this course of action might be a valid option. Also in view of total-body PET scanners (e.g. the Explorer project; Badawi *et al* 2019) a cheap high-performance scintillator delivering excellent timing, might compensate in part for a loss in sensitivity (Moskal *et al* 2016, 2019). The problem of light transport in high-aspect-ratio crystals could be solved, for instance, by reading out the crystals on the long side (Cates and Levin 2018). One could also combine the excellent timing performance of cross-luminescence (e.g. in BaF$_2$) read out by VUV-SiPMs with the high detection efficiency of

heavy scintillators (e.g. BGO). This could simply be done by placing BaF_2 in front of BGO. In this approach Compton scattering (or full gamma absorption) in BaF_2 would provide excellent timing while BGO could provide the sensitivity. This idea is especially interesting in systems with crystal matrices, as it could work as a Compton camera, providing additional benefits not accessible nowadays in standard TOF-PET detectors. A further approach could be to produce energy-sharing sampling pixels with thin slabs of BaF_2 alternating with BGO, similar to the work in Turtos *et al* (2019a), but placing the SiPM on the side. The excellent PDE of the VUV-SiPMs in the visible range would further allow us to read the BGO light with no need for additional costly infrastructure. With advanced electronics, one could even make use of Cherenkov emission in BGO (Gundacker *et al* 2019, Kratochwil *et al* 2020) in order to improve the overall timing in both approaches. These are just a few examples of how the excellent timing of low-density materials can be combined with the high stopping power of other materials in order to gain the best of both worlds.

Nevertheless, aggressive and challenging research on photodetectors as well as on scintillator material is still needed to achieve sub-30 ps timing in TOF-PET. This includes the readout electronics, since many new developments such as high-frequency signal treatment have still not been implemented in application specific integrated circuits (ASICs). However, the high photon time density, defined as N/τ_d (Gundacker and Heering 2020) of cross-luminescence emission might also give an advantage in the front-end signal-to-noise ratio and power consumption. It is well known that the bandwidth and speed of the front-end, defining the signal slew-rate (dV/dt), is strongly correlated with the power uptake. On the other hand, a fast scintillator with a high photon time density also increases dV/dt. Due to this fact, it can be shown that the electronic part of the time resolution is proportional to the inverse scintillation photon time density ($CTR_{electr.} \propto \tau_d/N$) with a given decay time τ_d and number of photons detected N. The contribution of the scintillation statistics, on the other hand, is proportional to the square root of the inverse photon time density ($CTR_{photost.} \propto \sqrt{\tau_d/N}$) (Gundacker *et al* 2020). As a consequence, the electronic bandwidth and noise become less important with increasing photon time density. Nowadays, the market offers several ASICs, for example the TOFPET2 ASIC from PETsys (Francesco *et al* 2016), NINO-ASIC (Anghinolfi *et al* 2004, Powolny *et al* 2011), FlexTOT (Comerma *et al* 2013, Sarasola *et al* 2017), PETA-ASIC (Fischer *et al* 2009, Piemonte *et al* 2013), STiC3 (Stankova *et al* 2015), PETIROC (Fleury *et al* 2014) and many more. For modern ASICs the use of ultrafast cross-luminescence, read out by VUV-SiPMs, could give the best achievable time resolution, subject to many exciting future studies.

6. Conclusion

We have shown that VUV-sensitive SiPMs from FBK can be successfully applied for the readout of fast cross-luminescence emission in BaF_2. Using these photodetectors we have further investigated ultrafast emission in BaF_2 with a scintillation decay time below 100 ps. This fast almost prompt scintillation component, tentatively assigned to a quenched cross-luminescence due to energy transfer to simultaneously created electronic excitations, is of the greatest interest for fast timing applications in TOF-PET and HEP. However, the scintillation light transfer to the photodetector has to be as efficient as possible. In this regard, the coupling of the crystal to the SiPM remains a challenge, with many experimental difficulties , both known and still to be discovered. Furthermore, the Teflon wrapping used might be insufficient and future studies should focus on improved wrapping and optical coupling agents.

Nevertheless, we revealed a best achieved CTR of 51 ps FWHM for 2 mm × 2 mm × 3 mm crystals from Epic Crystal wrapped in Teflon, coupled with glycerine to VUV-HD SiPMs from FBK. This constitutes a new state-of-the-art timing with inorganic scintillators, compared with the best achieved CTR of 58 ps FWHM using LSO:Ce:Ca crystals of similar dimensions read out by FBK NUV-HD SiPMs. Improvements of the VUV-SiPM PDE, at present only 22%, to values as high as the 59% seen in the FBK NUV-HD SiPMs for LYSO:Ce emission, would boost the CTR of BaF_2 even further into the 20 ps FWHM range.

Doping of BaF_2 can effectively eliminate the slow ~800 ns decay time component originating from STE emission, and opens the door to ultrafast high-rate applications with gigahertz repetition rates. This is significant for instance in beam dose monitoring for hadron therapy, HEP, single x-ray CT or high-rate PET. We further observed that such doping has almost no influence on the fast cross-luminescence emission intensity and its lifetime, especially not the ultrafast component with decay times below 100 ps.

Working on improving the SPTR of SiPMs (from state-of-the-art values of 70 ps FWHM towards 10 ps FWHM) could further boost the CTR by making best use of this ultrafast, almost prompt, emission in BaF_2. In this respect, envisaging ambitious R&D on VUV-SiPMs could make the seemingly impossible dream of a 10 ps TOF-PET scanner (Schaart *et al* 2020) possible via, cross-luminescence detection (e.g. using BaF_2 crystals).

Acknowledgments

ORCID iDs

S Gundacker ⓘ https://orcid.org/0000-0003-2087-3266
R H Pots ⓘ https://orcid.org/0000-0002-5286-7357
R Shendrik ⓘ https://orcid.org/0000-0001-6810-8649

References

Acerbi F and Gundacker S 2019 Understanding and simulating SiPMs *Nucl. Instrum. Methods Phys. Res.* A **926** 16–35

Aleksandrov Y M, Makhov V N, Rodnyi P A, Syreishchikova T I and Yakimenko M N 1984 Intrinsic luminescence of BaF_2 at pulse excitation by synchrotron radiation *Sov. Phys. Solid State* **26** 2865–7

Allemand R, Gresset C and Vacher J 1980 Potential advantages of a cesium fluoride scintillator for a time-of-flight positron camera *J. Nucl. Med.* **21** 153–5

Anghinolfi F, Jarron P, Krummenacher F, Usenko E and Williams M C S 2004 NINO: an ultrafast low-power front-end amplifier discriminator for the time-of-flight detector in the ALICE experiment *IEEE Trans. Nucl. Sci.* **51** 1974–8

Badawi R D *et al* 2019 First human imaging studies with the explorer total-body PET scanner *J. Nucl. Med.* **60** 299–303

Bell Z W 2012 Scintillation counters *Handbook of Particle Detection and Imaging* ed C Grupen and I Buvat 2nd edn (Berlin: Springer) ch 15 pp 349–75

Bruyndonckx P, Liu X, Tavernier S and Zhang S 1997 Performance study of a 3D small animal pet scanner based on BaF_2 crystals and a photo sensitive wire chamber *Position-Sensitive Detectors Conf. 1996; Nucl. Instrum. Methods Phys. Res.* A **392** 407–13

Cates J W, Gundacker S, Auffray E, Lecoq P and Levin C S 2018 Improved single photon time resolution for analog SiPMs with front end readout that reduces influence of electronic noise *Phys. Med. Biol.* **63** 185022

Cates J W and Levin C S 2018 Evaluation of a clinical TOF-PET detector design that achieves $\leqslant$ 100 ps coincidence time resolution *Phys. Med. Biol.* **63** 115011

Chen J, Yang F, Zhang L, Zhu R, Du Y, Wang S, Sun S and Li X 2018 Slow scintillation suppression in yttrium doped BaF_2 crystals *IEEE Trans. Nucl. Sci.* **65** 2147–51

Comerma A, Gascón D, Freixas L, Garrido L, Graciani R, Marín J and Martínez G 2013 Flextot—current mode ASIC for readout of common cathode SiPM arrays *2013 IEEE Nucl. Sci. Symp. and Med. Imaging Conf. (2013 NSS/MIC) (Seoul, Korea South, 27 October–November 2013)* pp 1–2

Defrise M, Rezaei A and Nuyts J 2012 Time-of-flight PET data determine the attenuation sinogram up to a constant *Phys. Med. Biol.* **57** 885–99

Derenzo S 2008 *The quest for new radiation detector materials*

Derenzo S E, Weber M J, Moses W W and Dujardin C 2000 Measurements of the intrinsic rise times of common inorganic scintillators *IEEE Trans. Nucl. Sci.* **47** 860–4

Dorenbos P, de Haas J, Visser R, Eijk C W V and Hollander R 1992 Absolute light yield measurements on BaF_2 crystals and the quantum efficiency of several photomultiplier tubes *IEEE Trans. Nucl. Sci.* **40** 424–30

Ershov N N, Zakharov N G and Rodnyi P A 1982 Spectral-kinetic study of the intrinsic-luminescence characteristics of a fluorite-type crystal *Opt. Spectrosc.* **53** 51–4

Fischer P, Peric I, Ritzert M and Koniczek M 2009 Fast self triggered multi channel readout ASIC for time- and energy measurement *IEEE Trans. Nucl. Sci.* **56** 1153–8

Fleury J, Callier S, de La Taille C, Seguin N, Thienpont D, Dulucq F, Ahmad S and Martin G 2014 Petiroc and citiroc: front-end ASICs for SiPM read-out and ToF applications *J. Instrum.* **9** C01049–01049

Francesco A D, Bugalho R, Oliveira L, Rivetti A, Rolo M, Silva J C and Varela J 2016 Tofpet 2: a high-performance circuit for PET time-of-flight *Nucl. Instrum. Methods Phys. Res.* A **824** 194–5

Gola A, Acerbi F, Capasso M, Marcante M, Mazzi A, Paternoster G, Piemonte C, Regazzoni V and Zorzi N 2019 NUV-sensitive silicon photomultiplier technologies developed at fondazione Bruno Kessler *Sensors* **19**

Gundacker S, Auffray E, Frisch B, Jarron P, Knapitsch A, Meyer T, Pizzichemi M and Lecoq P 2013 Time of flight positron emission tomography towards 100 ps resolution with L(Y) *J. Instrum.* **8** P07014

Gundacker S, Auffray E, Pauwels K and Lecoq P 2016 Measurement of intrinsic rise times for various L(Y)SO and LuAG scintillators with a general study of prompt photons to achieve 10 ps in TOF-PET *Phys. Med. Biol.* **61** 2802–37

Gundacker S and Heering A 2020 The silicon photomultiplier: fundamentals and applications of a modern solid-state photon detector *Phys. Med. Biol.* **65** 17TR01

Gundacker S, Knapitsch A, Auffray E, Jarron P, Meyer T and Lecoq P 2014 Time resolution deterioration with increasing crystal length in a TOF-PET system *Nucl. Instrum. Methods Phys. Res.* A **737** 92–100

Gundacker S, Turtos R M, Auffray E and Lecoq P 2018 Precise rise and decay time measurements of inorganic scintillators by means of x-ray and 511 keV excitation *Nucl. Instrum. Methods Phys. Res.* A **891** 42–52

Gundacker S, Turtos R M, Auffray E, Paganoni M and Lecoq P 2019 High-frequency SiPM readout advances measured coincidence time resolution limits in TOF-PET *Phys. Med. Biol.* **64** 055012

Gundacker S, Turtos R M, Kratochwil N, Pots R H, Paganoni M, Lecoq P and Auffray E 2020 Experimental time resolution limits of modern SiPMs and TOF-PET detectors exploring different scintillators and Cherenkov emission *Phys. Med. Biol.* **65** 025001

Hu C, Zhang L, Zhu R, Chen J, Ding D, Wang Y and Zhang M 2020 Spatial resolution of an inorganic crystal-based hard x-ray imager *IEEE Trans. Nucl. Sci.* **67** 1014–9

Hu C, Zhang L, Zhu R-Y, Demarteau M, Wagner R, Xia L, Xie J, Li X, Wang Z, Shih Y and Smith T 2019 Ultrafast inorganic scintillator-based front imager for gigahertz hard x-ray imaging *Nucl. Instrum. Methods Phys. Res.* A **940** 223–9

Ishii K, Orihara H, Matsuzawa T, Binkley D M and Nutt R 1990 High resolution time-of-flight positron emission tomograph *Rev. Sci. Instrum.* **61** 3755–62

Kamenskikh I, Tishchenko E, Kirm M, Omelkov S, Belsky A and Vasil'ev A 2020 Decay kinetics of CeF_3 under VUV and x-ray synchrotron radiation *Symmetry* **12** 914

Kirm M, Andrejczuk A, Krzywinski J and Sobierajski R 2005 Influence of excitation density on luminescence decay in $Y_3Al_5O_{12}$:Ce and BaF_2 crystals excited by free electron laser radiation in VUV *Phys. Status Solidi* c **2** 649–52

Kirm M, Vielhauer S, Zimmerer G, Lushchik A and Lushchik C 2002 Cation and anion electronic excitations in MgO and BaF_2 crystals under excitation by photons up to 75 eV *Surf. Rev. Lett.* **9** 1363–8

Kratochwil N, Gundacker S, Lecoq P and Auffray E 2020 Pushing Cherenkov PET with BGO via coincidence time resolution classification and correction *Phys. Med. Biol.* **65** 115004

Laval M, Allemand R, Campagnolo R, Garderet P, Gariod R, Guinet P, Moszinski M, Tournier E and Vacher J 1982 Contribution of the time-of-flight information to the positron tomographic imaging *Proc. 3rd World Congress Nucl. Med. and Biol.* 3 *(Paris, France 29 August–2 September 1982)* (Oxford: Pergamon) pp 2315–23

Laval M, Moszynski M, Allemand R, Cormoreche E, Guinet P, Odru R and Vacher J 1983 Barium fluoride—inorganic scintillator for subnanosecond timing *Nucl. Instrum. Methods Phys. Res.* **206** 169–76

Lecoq P, Gektin A and Korzhik M 2017 *Inorganic Scintillators for Detector Systems* 2nd edn (Berlin: Springer) 3

Lecoq P *et al* 2020 Roadmap toward the 10 ps time-of-flight PET challenge *Phys. Med. Biol.* **65**

Lewellen T K, Bice A N, Harrison R L, Pencke M D and Link J M 1988 Performance measurements of the SP3000/UW time-of-flight positron emission tomograph *IEEE Trans. Nucl. Sci.* **35** 665–9

Li H H 1980 Refractive index of alkaline earth halides and its wavelength and temperature derivatives *J. Phys. Chem. Ref. Data* **9** 161–290

Malitson I H 1964 Refractive properties of barium fluoride *J. Opt. Soc. Am.* **54** 628–32

Moskal P *et al* 2016 Time resolution of the plastic scintillator strips with matrix photomultiplier readout for j-PET tomograph *Phys. Med. Biol.* **61** 2025–47

Moskal P *et al* 2019 Feasibility study of the positronium imaging with the j-PET tomograph *Phys. Med. Biol.* **64** 055017

Mullani N A, Ficke D C, Hartz R, Markham J and Wong G 1981 System design of fast pet scanners utilizing time-of-flight *IEEE Trans. Nucl. Sci.* **28** 104–8

Nepomnyashchikh A, Radzhabov E, Egranov A and Ivashechkin V 2001 Luminescence of BaF_2-LaF_3 *Radiat. Meas.* **33** 759–62

Nepomnyashchikh A, Radzhabov E, Egranov A, Ivashechkin V and Istomin A 2002 Recombination processes in crystals of solid solutions of $Ba_{1-x}La_xF_{2x}$ *Nucl. Instrum. Methods Phys. Res.* A **486** 390–4

Nepomnyashchikh A, Radzhabov E, Egranov A, Ivashechkin V, Istomin A and Kurobori T 2005 Defect formation in BaF2 crystals doped with cadmium *Nucl. Instrum. Methods Phys. Res.* A **537** 27–30

Omelkov S I, Nagirnyi V, Gundacker S, Spassky D A, Auffray E, Lecoq P and Kirm M 2018 Scintillation yield of hot intraband luminescence *J. Lumin.* **198** 260–71

Pankratov V *et al* 2019 Progress in development of a new luminescence setup at the FinEstBeAMS beamline of the MAX IV laboratory *Radiat. Meas.* **121** 91–8

Pärna R *et al* 2017 FinEstBeaMS—a wide-range Finnish-Estonian beamline for materials science at the 1.5 GeV storage ring at the MAX IV Laboratory *Nucl. Instrum. Methods Phys. Res.* A **859** 83–9

Piemonte C, Gola A, Tarolli A, Fisher P, Ritzert M, Schulz V and Solf T 2013 Performance of FBK SiPMs coupled to PETA3 read-out ASIC for PET application *Nucl. Instrum. Methods Phys. Res.* A **718** 345–6

Pots R H, Auffray E and Gundacker S 2020 Exploiting cross-luminescence in BaF_2 for ultrafast timing applications using deep-ultraviolet sensitive HPK silicon photomultipliers *Front. Phys.* **8** 482

Powolny F *et al* 2011 Time-based readout of a silicon photomultiplier (SiPM) for time of flight positron emission tomography (TOF-PET) *IEEE Trans. Nucl. Sci.* **58** 597–604

Radzhabov E, Istomin A, Nepomnyashikh A, Egranov A and Ivashechkin V 2005 Exciton interaction with impurity in barium fluoride crystals *Nucl. Instrum. Methods Phys. Res.* A **537** 71–5

Radzhabov E and Kirm M 2005 Triplet luminescence of cadmium centres in alkaline-earth fluoride crystals *J. Phys.: Condens. Matter* **17** 5821–30

Radzhabov E, Kirm M, Egranov A, Nepomnyachshikh A and Myasnikova A 2006 A mechanism of exciton suppression in alkaline-earth fluorides doped with La, Y, Cd *Proc. SCINT 2005* pp 60–3

Radzhabov E, Nepomnyashchikh A and Kirm M 2007 Optical transitions in pairs of trivalent ion-interstitial fluorine in alkaline-earth fluorides *Phys. Status Solidi* A **204** 670–6

Radzhabov E, Shalaev A and Nepomnyashikh A 1998 Exciton luminescence suppression in BaF_2-LaF_3 solid solutions *Radiat. Meas.* **29** 307–9

Radzhabov E A, Kirm M, Egranov A and Nepomnyaschikh A 2008 Energy dissipation in impurity doped alkaline-earth fluorides *IEEE Trans. Nucl. Sci.* **55** 1123–7

Rodnyi P, Terekhin M and Mel'chakov E 1991 Radiative core-valence transitions in barium-based fluorides *J. Lumin.* **47** 281–4

Rossignol J, Turtos R M, Gundacker S, Gaudreault D, Auffray E, Lecoq P, Bérubé-Lauzière Y and Fontaine R 2020 Time-of-flight computed tomography—proof of principle *Phys. Med. Biol.* **65** 085013

Sarasola I, Nemallapudi M, Gundacker S, Sánchez D, Gascón D, Rato P, Marín J and Auffray E 2017 A comparative study of the time performance between NINO and FlexToT ASICs *J. Instrum.* **12** P04016

Sarukura N, Nawata T, Ishibashi H, Ishii M and Fukuda T 2015 Czochralski growth of oxides and fluorides *Handbook of Crystal Growth* ed P Rudolph 2nd edn (Boston: Elsevier) pp 131–68

Schaart D R, Ziegler S and Zaidi H 2020 Achieving 10 ps coincidence time resolution in TOF-PET is an impossible dream *Med. Phys.* **47** 2721–4

Shendrik R and Radzhabov E 2014 Absolute light yield measurements on SrF$_2$ and BaF$_2$ doped with rare earth ions *IEEE Trans. Nucl. Sci.* **61** 406–10

Stankova V, Shen W, Briggl K, Chen H, Fischer P, Gil A, Harion T, Kiworra V, Munwes Y, Ritzert M and Schultz-Coulon H-C 2015 STIC3— silicon photomultiplier timing chip with picosecond resolution *Nucl. Instrum. Methods Phys. Res.* A **787** 284–7

Terekhin M A, Vasil'ev A N, Kamada M, Nakamura E and Kubota S 1995 Effect of quenching processes on the decay of fast luminescence from barium fluoride excited by VUV synchrotron radiation *Phys. Rev.* B **52** 3117–21

Ter-Pogossian M M, Ficke D C, Yamamoto M and Hood J T 1982 Super PETT I: a positron emission tomograph utilizing photon time-of-flight information *IEEE Trans. Med. Imaging* **1** 179–87

Turtos R M, Gundacker S, Auffray E and Lecoq P 2019a Towards a metamaterial approach for fast timing in PET: experimental proof-of-concept *Phys. Med. Biol.* **64** 185018

Turtos R M *et al* 2019b On the use of CdSe scintillating nanoplatelets as time taggers for high-energy gamma detection *Npj 2D Mater. Appl.* **3**

van Eijk C 1994 Cross-luminescence *J. Lumin.* **60–61** 936–41

Vasil'ev A N, Kolobanov V N and Kuusman I L 1985 Multiplication of electronic excitations in MgO crystals *Fiz. Tverd. Tela* **27** 2696–702

Vinogradov S 2017 Approximations of coincidence time resolution models of scintillator detectors with leading edge discrimination *Nucl. Instrum. Methods Phys. Res.* A **912** 149–53

Zhu R-Y 2015 The next generation of crystal detectors *J. Phys.: Conf. Ser.* **587** 012055